An extended Kalman filter for fetal heart location estimation during Doppler-based heart rate monitoring

An Extended Kalman Filter for Fetal Heart Location Estimation During Doppler-Based Heart Rate Monitoring

Paul Hamelmann, Rik Vullings, Massimo Mischi, *Senior Member, IEEE*, Alexander F. Kolen, Lars Schmitt, and Jan W. M. Bergmans

***Abstract*— Fetal heart rate (fHR) monitoring using the Doppler ultrasound (US) is a standard clinical practice for assessing fetal well-being before and during labor. For continuous fHR measurements, the US transducer is positioned on the maternal abdomen using a flexible belt. Due to fetal movement, the relative fetal heart location (fHL) with respect to the US transducer can change, leading to frequent periods of signal loss hampering the clinical assessment of fetal health. Consequently, the clinical staff has to repeatedly reposition the US transducer—a cumbersome task affecting clinical workflow. We propose a method to estimate the fHL during fHR monitoring to support clinicians in efficiently repositioning the US transducer. Unlike typical US transducers, which do not provide any information on the spatial fHL, we exploit the fact that multiple transducer elements are present in the array aperture of the US transducer. We developed a novel model that relates the measured Doppler power in the individual transducer elements to the fHL and use it within the probabilistic framework of an extended Kalman filter (EKF). The performance of the EKF algorithm was evaluated in simulations and in *in vitro* experiments using a dedicated setup of a beating fetal heart. Both simulations and *in vitro* experiments showed that the fHL can be determined with an accuracy of 4 mm. Furthermore, we demonstrate that when the fetal heart is drifting out of the US beam, the EKF algorithm accurately estimates the fHL up to a radial distance of 34 mm.**

***Index Terms*— Doppler ultrasound (US), extended Kalman filter (EKF), fetal heart rate (fHR), location estimation.**

I. Introduction

CARDIOTOCOGRAPHY (CTG), the continuous registration of fetal heart rate (fHR) and uterine contractions, is a standard method in clinical practice to assess the fetal well-being [2]. A common way to measure the fHR during the antepartum and intrapartum period is by means of Doppler ultrasound (US). For that, a US transducer, operating in a pulsed-wave Doppler mode, is positioned on the maternal abdomen and directed toward the fetal heart location (fHL).

Manuscript received July 25, 2018; revised September 30, 2018; accepted October 01, 2018. Date of publication November 14, 2018; date of current version August 9, 2019. The Associate Editor coordinating the review process was José Pereira. *(Corresponding author: Paul Hamelmann.)*

P. Hamelmann, R. Vullings, M. Mischi, and J. W. M. Bergmans are with the Department of Electrical Engineering, Eindhoven University of Technology, 5612 AP Eindhoven, The Netherlands (e-mail: p.c.hamelmann@tue.nl).

A. F. Kolen and L. Schmitt are with Philips Research, 5656 AE Eindhoven, The Netherlands.

Color versions of one or more of the figures in this paper are available online at http://ieeexplore.ieee.org.

Digital Object Identifier 10.1109/TIM.2018.2876779

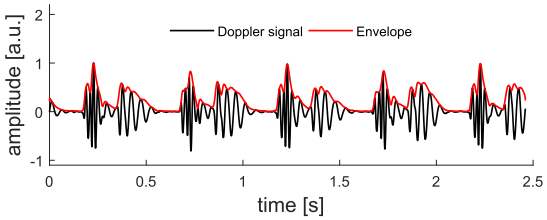

Fig. 1. Example of a Doppler signal measured in *in vitro* experiments using a commercially available US transducer (Philips Avalon, Philips Medizin-Systeme Böblingen GmbH, Germany). The fHR is estimated from the Doppler signal by determining the periodicity of the envelope signal using an autocorrelation approach.

From the received US echoes, a Doppler signal is generated, representing the motion due to the contracting heart ventricles, valve movement, and blood flow [20]. This Doppler signal is, after detection of its envelope, further processed using autocorrelation approaches in which the signal periodicity is determined as a surrogate for the fHR [10], [18]. The majority of commercially available CTG US transducers consist of multiple transducer elements distributed over a surface of several centimeters to increase the measurement volume in which the fHR can be determined. In order to reduce the required processing complexity, the received US signals in the individual elements are typically combined and then one Doppler signal is generated, from which the fHR is estimated [18], [21]. In that way, effectively, the array aperture is treated as a single-element transducer. In Fig. 1, a Doppler signal acquired with a commercially available CTG US transducer is shown.

In recent studies, the added value of having multiple transducer elements is further exploited. In [12], a multigate sensor system is described in which for each transducer element a Doppler signal from various depth is determined, with the objective of identifying different fetal movements. Furthermore, in [22], the potential of a multi-Doppler system is used to improve the robustness of fHR estimation.

In clinical practice, after positioning the US transducer on the maternal abdomen, a flexible belt holds the transducer in the place. However, during the long lasting continuous measurement sessions, it frequently happens that the fHL changes with respect to the US transducer. This can be either due to a displacement of the US transducer on the maternal

abdomen or due to a change of fHL within the uterus. For robust fHR measurement, it is necessary that the fetal heart is located within the US beam of the transducer. Therefore, before positioning the US transducer on the maternal abdomen, the clinical staff palpates in order to establish the fetal position. In addition, the auditive feedback of the Doppler signal guides the staff in finding a suitable US transducer position. Depending on the experience of the clinician, the gestational age of the fetus and the body mass index (BMI) of the mother, this can be a very challenging task and may strongly impact the clinical workflow. Therefore, in [8], we introduced a method to alleviate this problem by providing additional information on the fHL with respect to the US transducer to aid clinicians with this cumbersome task. This method inferred the fHL from the Doppler power, measured with a commercially available seven-element US transducer, by separately analyzing the seven transducer-element Doppler signals using a maximum likelihood (ML) estimation approach.

The accuracy of this method is mainly limited by the signal-to-noise ratio (SNR) of the Doppler power measurements. In clinical practice, US measurements on mothers with a high BMI often show a reduced SNR due to high US attenuation by fatty tissue compared to measurements on mothers with a low or moderate BMI [17]. Therefore, the objective of this research is to further improve the performance of the fHL estimation, such that the method of aiding clinicians with the positioning of the US transducer on the maternal abdomen can also be applied in measurements with a low SNR. Supporting clinicians with the positioning of the US transducer on the maternal abdomen eventually may lead to more robust measurements of fHR.

By including the *prior* knowledge on the fHL into the derivation of the method presented in [8], improved fHL estimation may be achieved. Here, the fact is used that the fHL can only change gradually over time. Gradually changing parameters are recognized in many different application areas and it is known that a Kalman filter (KF) is an effective method to estimate those parameters in the presence of Gaussian distributed measurement noise [4]. Within the field of fHR monitoring, Kalman filtering has shown its potential by successfully estimating maternal signals to extract the fHR in electrocardiographic recordings [1].

In Section II, we derive a KF suitable for estimating the fHL. The resulting fHL estimation algorithm is evaluated using simulations and *in vitro* measurements and compared to the ML estimation presented in [8]. The results of this evaluation are presented in Section III and discussed in Section IV. This paper concludes with a recap on the main results and their clinical significance in Section V.

II. Materials and Methods

A. System Characterization

When a transmitted US wave travels through the maternal abdomen, it is reflected by various structures, which is then received by the individual elements of the US transducer. In this research, a commercially available US transducer (Philips Avalon, Philips Medizin-Systeme Böblingen GmbH, Germany) is used. The array aperture of this transducer consists of six transducer elements circularly arranged around one center element with a pitch of 2 cm (see Fig. 2). By individually soldering each transducer element of the US transducer via coaxial cables to an open US platform (Vantage 256, Verasonics, Inc., Kirkland, WA, USA), separate control of the elements in transmission and receive mode is enabled. The received US signals in the individual elements will show the reflections of many other structures and not only those of the fetal heart. Therefore, it is not possible to directly infer the fHL from the received US signals. Therefore, for each transducer element, a Doppler signal is derived. These Doppler signals contain only information related to moving structures, ideally only the fetal heart, within the sample volume (SV). The frequency content of these Doppler signals is determined by the velocity of the moving structures within the SV and the insonification angle [3], [20]. The amplitude of the Doppler signal depends on the fHL within the radiation pattern. Due to the fact that the heart is beating, there will be periods in which there is no movement at all. Therefore, the power P_i of the Doppler signals measured in each transducer element, indicated by the index i, is calculated in a time window W. It is important that W is chosen long enough, such that at least one heartbeat is contributing to the Doppler power P_i.

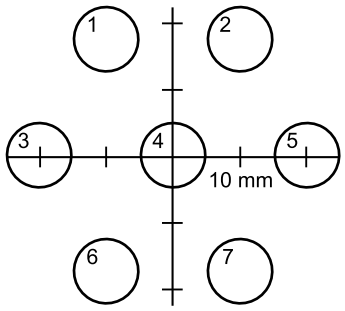

Fig. 2. Array aperture of the employed US transducer containing seven transducer elements.

The strength of the received Doppler power P_i is then directly dependent on where the fetal heart, indicated by the position vector $\mathbf{h} = [h_x, h_y, h_z]$, is located within the radiation pattern Ψ_i of the employed US transducer. Here, the index i denotes the number of an individual transducer element. When the fetal heart is directly located within Ψ_i of a specific transducer element, the Doppler power P_i of that element will be high compared to the other transducer elements. The transmit-receive radiation pattern Ψ_i was characterized in [8] by measuring the transmit-radiation pattern using a needle hydrophone setup. In order to account for the fetal heart dimension, the radiation pattern Ψ_i was integrated over the insonified surface of the fetal heart, yielding a spatial distribution Φ_i. We chose to model the insonified surface of the heart as a disc with diameter $d_h = 3.5$ cm, which corresponds to the average size of the fetal heart at a gestational age of 40 weeks [14]. A detailed description of the characterization of Φ_i can be found in [8].

We can model the received Doppler power P_i as

$$P_i(\mathbf{h}) = \alpha \Phi_i(\mathbf{h}) + \mathbf{v}_i. \tag{1}$$

Due to the fact that Φ_i does not provide any information on the absolute value of P_i, a scaling factor α is included in the model. This scaling factor accounts for various factors such as attenuation, the driving voltage of the transmitting element or the window length, W, in which the power is calculated. Besides that, when there are more heart beats within the window W, a higher power will be measured. It is assumed that α is equal for all transducer elements since its value is affected by factors which are assumed to be approximately the same for all elements. The measurement noise is described by $\mathbf{v}_i$.

B. Measurement Noise Modeling

For the derivation of the extended KF (EKF) equations in Section II-D, it is useful to assume that the measurement noise $\mathbf{v}_t$ is distributed with zero mean and covariance matrix $\mathbf{R}_t$.

However, as the Doppler power can never be negative, it can directly be recognized that describing $\mathbf{v}_t$ with a normal distribution with zero mean is not a valid noise model. Instead, rather than the noise in the Doppler power, it is more realistic to model the noise in the raw Doppler signal with a normal distribution with covariance σ^2 [6]. Due to the fact that the power is calculated by computing the mean squared value in a window W with N samples of the Doppler signal, $\mathbf{v}_t$ can be described using a gamma distribution with shape parameter $k = N/2$ and scale parameter $\theta = 2\sigma^2/N$ [13]. The fact that N is relatively large allows us again to approximate this gamma distribution with a normal distribution with covariance $2\sigma^4/N$ centered around the mean σ^2 [13]. This means that the noise in the Doppler signal adds a constant offset value to the modeled Doppler power in (1). Accordingly, we can rewrite the power model as

$$P_i(\mathbf{h}) = \alpha\Phi(\mathbf{h}) + \sigma^2 + \mathbf{v}' \tag{2}$$

where $\mathbf{v}'$ is distributed with $\mathbf{v}' \sim \mathcal{N}(0, \mathbf{R})$.

C. State-Space Representation

During fHR measurement sessions, the fetus and, consequently, the fetal heart can move within the maternal uterus up to a certain degree freely. However, it is valid to assume that the location of the heart does not change abruptly between two subsequent time points, but follows a smooth trajectory, provided that the time interval is sufficiently small. Therefore, it is chosen to model the fHL $\mathbf{h}$ with a first-order Gauss–Markov process with process noise $\mathbf{d}_t$, having zero mean and covariance matrix $\mathbf{Q}_t$. The magnitude of the covariance matrix $\|\mathbf{Q}_t\|$ determines the possible change of $\mathbf{h}$ in between two subsequent time points t and $t+1$. It is assumed that $\mathbf{Q}_t$ is a diagonal matrix with equal values on the diagonal, meaning that there is no preferred direction in which the fetal heart moves. Accordingly, the change of $\mathbf{h}$ can then be described using a state-space model representation (see also Fig. 3)

$$\begin{aligned} \mathbf{h}_{t+1} &= \mathbf{h}_t + \mathbf{d}_t \\ \mathbf{P}_t &= \mathbf{g}(\mathbf{h}_t) + \mathbf{v'}_t \end{aligned} \tag{3}$$

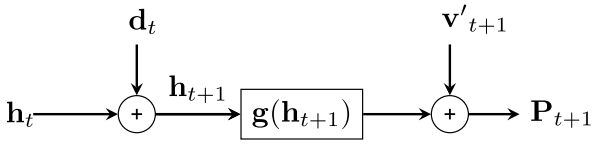

Fig. 3. Illustration of the state-space model.

where $\mathbf{P}_t$ is a vector of the Doppler power P_i measured in the individual elements at time t. For the sake of readability, we denote the modeled power in (1), without the noise term $\mathbf{v'}_t$, as the nonlinear function $\mathbf{g}(\mathbf{h}_t) = \alpha\Phi(\mathbf{h}) + \sigma^2$ which maps the fHL $\mathbf{h}_t$ into the domain of the power measurements $\mathbf{P}_t$.

D. Derivation of the Extended Kalman Filter

The probabilistic nature of the noisy sequence of power measurements and the uncertainty in the state-space model (3) encourages us to estimate $\mathbf{h}$ using a statistical analysis and we choose to follow a Bayesian approach. The conditional *posterior* probability, describing the probability that the fHL is true given the measured power $\mathbf{P}$, can be expressed using Bayes' theorem

$$\begin{aligned} &p(\mathbf{h}_{t+1}|\mathbf{P}_{t+1}, \mathbf{Q}_t, \mathbf{R}_t) \\ &\qquad = \frac{p(\mathbf{P}_{t+1}|\mathbf{h}_{t+1}, \mathbf{Q}_t, \mathbf{R}_t)\, p(\mathbf{h}_{t+1}|\mathbf{P}_t, \mathbf{Q}_t, \mathbf{R}_t)}{p\,(\mathbf{P}_{t+1}|\mathbf{P}_t, \mathbf{Q}_t, \mathbf{R}_t)}. \end{aligned} \tag{4}$$

The conditional probabilities in the numerator of the right-hand side of (4) are referred to as *likelihood* and prior, respectively. The conditional probability in the denominator is referred to as the *evidence*. Because we assume that the measurement noise and the process noise are distributed normally, from (4), one can derive the well-known KF equations for the fHL $\mathbf{h}_{t+1}$ and its covariance $\mathbf{S}_{t+1}$ [4]. In order to denote an estimated parameter, we use a tilde, e.g., $\tilde{\mathbf{h}}_{t+1}$. Because $\mathbf{g}$ is a nonlinear function, the KF equations can be extended by linearizing $\mathbf{g}$ around the current estimate of the fHL $\tilde{\mathbf{h}}_t$.

Accordingly, the full EKF equations are given by

$$\widetilde{\mathbf{h}}_{\mathbf{t+1}} = \widetilde{\mathbf{h}}_{\mathbf{t}} + \mathbf{K}_{\mathbf{t+1}}(\mathbf{P}_{t+1} - \mathbf{g}(\widetilde{\mathbf{h}}_t)) \tag{5}$$

$$\widetilde{\mathbf{S}}_{t+1} = \widetilde{\mathbf{S}}_t + \mathbf{Q}_t - \mathbf{K}_{t+1}\mathbf{G}_{t+1}(\widetilde{\mathbf{S}}_t + \mathbf{Q}_t) \tag{6}$$

where $\mathbf{K}_{t+1}$ is known as the Kalman gain

$$\mathbf{K}_{t+1} = \frac{(\mathbf{S}_t + \mathbf{Q}_t)\mathbf{G}_{t+1}^T}{\mathbf{R}_{t+1} + \mathbf{G}_{t+1}(\mathbf{S}_t + \mathbf{Q}_t)\mathbf{G}_{t+1}^T} \tag{7}$$

and $\mathbf{G}_{t+1}$ is the Jacobian matrix computed at the current estimate $\widetilde{\mathbf{h}}_t$

$$\mathbf{G}_{t+1} = \frac{\delta\mathbf{g}}{\delta\mathbf{h}_t}|_{\mathbf{h}_t = \widetilde{\mathbf{h}}_t}. \tag{8}$$

The Kalman gain $\mathbf{K}$ is a matrix which determines whether we should trust more the new measurement data or rely on the previous estimate $\tilde{\mathbf{h}}_t$. From (7), it follows that the Kalman gain will be equal to the inverse of the Jacobian matrix when the measurements are very accurate. This occurs when the measurement noise covariance matrix is the zero matrix

$\mathbf{R}_{t+1} = \mathbf{0}_M$, with M being the total number of transducer elements, or when $\|\mathbf{Q}_t\|$ is very large

$$\lim_{\substack{\mathbf{R_{t+1}}\to\mathbf{0_M} \\ \|\mathbf{Q}\|_t\to\infty}} \mathbf{K}_{t+1} = \mathbf{G}_{\mathbf{t+1}}^{-\mathbf{1}}. \tag{9}$$

Likewise, when $\|\mathbf{R}\|$ is large compared to the state variance $\mathbf{S}$ and the process noise variance $\mathbf{Q}$ or when the Jacobian $\mathbf{G}$ approaches the zero matrix, the Kalman gain $\mathbf{K}$ approaches the zero matrix

$$\lim_{\substack{\|\mathbf{R}\|_{t+1}\to\infty \\ \mathbf{G_{t+1}}\to\mathbf{0_{M,H}}}} \mathbf{K}_{t+1} = \mathbf{0}_{H,M}. \tag{10}$$

Here, $\mathbf{0}_{H,M}$ denotes a zeros matrix with dimensions H and M, where H describes the dimensions of the state vector $\mathbf{h}$. For the purpose of interpretation of the Kalman Gain, it is useful to compute the norm $\|\mathbf{KG}\|$ as it reflects a single scalar value between 0 and 1. When the norm $\|\mathbf{KG}\|$ is close to 0, the new fHL estimate will mainly rely on the previous estimate.

E. Nuisance Parameter Estimation

During each KF iteration, the two nuisance parameters α and σ^2 have to be known in order to infer $\tilde{\mathbf{h}}_t$ from (5). Therefore, we choose to follow a hierarchical approach where in the first level of the algorithm $\tilde{\mathbf{h}}_t$ is estimated using the EKF, and then, in the second level, the nuisance parameters are determined. At the nuisance parameter estimation level, $\tilde{\mathbf{h}}_t$ is assumed to be known. Furthermore, it is assumed that the prior probability in (4) is uniform and the measurements $\mathbf{P}$ are statistically independent. This allows us to estimate the nuisance parameters $\tilde{\alpha}$ and $\tilde{\sigma}^2$ by following a ML estimation approach using a similar derivation as done in [8]:

$$\begin{aligned}\widetilde{\alpha}, \widetilde{\sigma}^2 &= \arg\max_{a,\sigma^2}\left(-\sum_{i=1}^{M}(P_i - \alpha\Phi_i(\tilde{\mathbf{h}}_t) - \sigma^2)^2\right) \\ &= \arg\max_{a,\sigma^2} L \end{aligned} \tag{11}$$

where L denotes the likelihood function. The two nuisance parameters α and σ^2 can be estimated by finding a solution to $\delta L/\delta\alpha = 0$ and $\delta L/\delta\sigma^2 = 0$, respectively, yielding

$$\widetilde{\alpha} = \frac{\sum_{i=1}^{M} P_i \sum_{i=1}^{M} \Phi_i - M\sum_{i=1}^{M} P_i\Phi_i}{\left(\sum_{i=1}^{M}\Phi_i\right)^2 - M\sum_{i=1}^{M}\Phi_i^2} \tag{12}$$

$$\widetilde{\sigma}^2 = \frac{\sum_{i=1}^{M} P_i\Phi_i \sum_{i=1}^{M}\Phi_i - \sum_{i=1}^{M}\Phi_i^2 \sum_{i=1}^{M} P_i}{\left(\sum_{i=1}^{M}\Phi_i\right)^2 - M\sum_{i=1}^{M}\Phi_i^2}. \tag{13}$$

Having an estimate for σ^2 allows us to update the measurement noise covariance matrix $\mathbf{R}$ for the next EKF iteration according to

$$\mathbf{R_t} = \frac{2\sigma^4}{N}\mathbf{I}_M \tag{14}$$

where $\mathbf{I_M}$ denotes the identity matrix with dimension $M = 7$, corresponding to the total number of transducer elements.

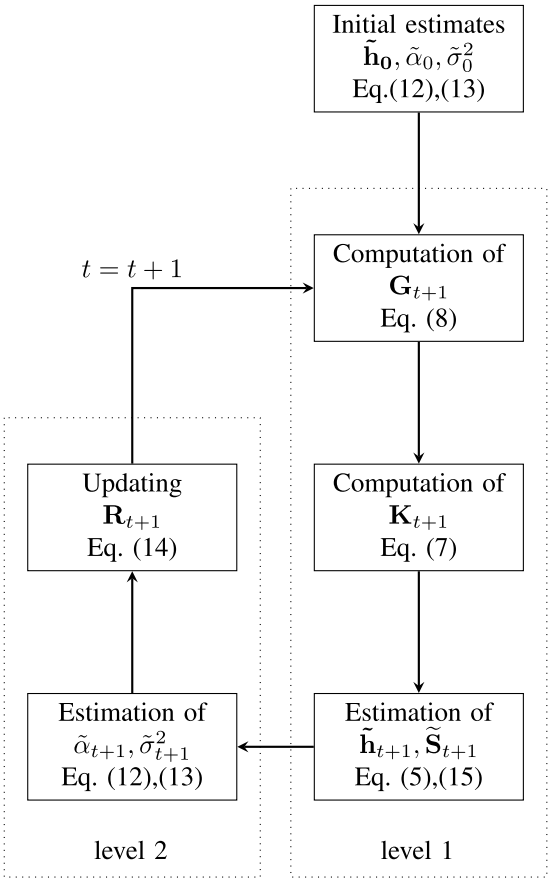

Fig. 4. Algorithmic implementation of the hierarchical fHL estimation algorithm. After initialization, the fHL is determined using the EKF. Thereupon, the nuisance parameters are estimated in the second level of the algorithm.

F. Algorithmic Implementation

In Fig. 4, the algorithmic implementation of the fHL estimation algorithm is schematically depicted. The EKF is initialized using the ML solution in (12) and (13). Then, in the first level of the hierarchical algorithm, the fHL is determined using the EKF. Numerical rounding errors during EKF iterations may cause the covariance matrix $\widetilde{\mathbf{S}}_{t+1}$ to lose its symmetry and positive definiteness. As a consequence, the EKF may diverge. This can be limited by implementing Joseph's form of the state variance update equation

$$\widetilde{\mathbf{S}}_{t+1} = \mathbf{A}\widetilde{\mathbf{S}}_t\mathbf{A}^T + \mathbf{K}_{t+1}\mathbf{R_t}\mathbf{K}_{t+1}^T \tag{15}$$

with $\mathbf{A} = \mathbf{I} - \mathbf{K}_{t+1}\mathbf{G}_{t+1}$ [11].

In the second level, the nuisance parameters are estimated. The estimation accuracy of the nuisance parameters is dependent on the quality of the power measurements and on the accuracy of $\tilde{\mathbf{h}}$. In case that the nuisance parameters have been estimated erroneously, large errors in the subsequent EKF iterations may occur since inference will be based on an incorrect model. In order to reduce the effect of possible outliers, it is chosen to take the temporal median value of the last five estimated nuisance parameters.

G. Measurement System

The commercially available US transducer (Philips Avalon, Philips Medizin-Systeme Böblingen GmbH, Germany) is

modified and its seven transducer elements are individually soldered to coaxial cables to establish a connection to an open US research platform (Vantage 256, Verasonics, Inc., Kirkland, WA, USA). This research platform provides individual control over the elements in transmission and receive mode. As described in a previous study, it is beneficial for the estimation of $\widetilde{\mathbf{h}}$ that the radiation pattern Ψ_i does not show too much interference because this allows one to link a measured power value P_i unambiguously to a specific fHL [7]. In order to avoid interference, only the center element ($i = 4$, see Fig. 2) of the array aperture is active in transmission. In the receive mode, all seven elements are active. For the transmission of a US wave, a center frequency $f_0 = 1$ MHz, pulse repetition frequency $PRF = 2$ kHz, and pulse duration $T = 10$ cycles are used. The driving voltage applied to the array aperture of the transducer was set to $V_{PP} = 5$ V. The raw reflected US waves are then received during an adjustable time window $\Delta\tau$, which defines the depth z and the size of the SV from which the Doppler signals are obtained [3]. The raw US signal is digitized using a sample frequency of $f_s = 4$ MHz and processed using a common IQ-demodulation scheme [9]. It should be noted that for each transmitted US wave, one sample of each Doppler signal is obtained, i.e., the sample frequency of the Doppler signals equals the pulse-repetition frequency (PRF). Subsequently, the Doppler power $\mathbf{P}$ is calculated using the mean squared value of the Doppler signals in a sliding time window $W = 1$ s with 20% overlap.

H. Simulations

The model in (2) allows us to simulate power values for various fHLs $\mathbf{h}$ and for different SNRs. Because the SNR is a function of the fHL, we have chosen to define the signal power as the mean power $\bar{\mathbf{P}}$ received by all elements when the fetal heart is directly located in the center of the radiation pattern, i.e., $\mathrm{SNR} = 10\log(\alpha\bar{\mathbf{P}}([0, 0, h_z])/\sigma^2)$. The simulations are used to analyze the performance of the EKF with regard to the following aspects in more detail as follows.

1) The performance of the EKF algorithm is affected by the magnitude of the chosen process noise covariance $\|\mathbf{Q}\|$, as it influences the Kalman gain $\mathbf{K}$ according to (7). In fact, for running the EKF, the only required parameter to set is the process noise variance because the measurement noise variance $\mathbf{R}$ is adaptively updated after each iteration (14). In order to determine the optimal settings for $\|\mathbf{Q}\|$, a change of fHL is simulated for varying velocities u. It was chosen to let the fetal heart move at a constant radial distance $\|\mathbf{h}\| = (h_x^2 + h_y^2)^{1/2}$ around the center of the radiation pattern. In that way, the SNR is approximately constant and the EKF performance is mainly affected by the selected process noise variance. In this simulation, after a short convergence period of 2 s, the heart moves two times around the center of the radiation pattern and the radial distance was set to $\|\mathbf{h}\| = 15$ mm. For all possible combinations of u, $\|\mathbf{Q}\|$, and SNR, the simulation was executed $k = 50$ times. The performance of the algorithm was then evaluated by taking the mean error, defined as the Euclidean distance between true and estimated heart location, i.e., $\text{error} = ((h_x - \tilde{h}_x)^2 + (h_y - \tilde{h}_y)^2)^{1/2}$.
2) With increasing noise level, a decrease in the nuisance parameter estimation accuracy is expected. In order to investigate the effect of decreasing SNR, the measured power is simulated for fHLs at increasing radial distance $\|\mathbf{h}\|$.
   The simulated SNR in each simulation determines the value for σ^2 while the scaling factor is set constant to $\alpha = 1$. For each radial distance $\|\mathbf{h}\|$, the simulation is executed $k = 50$ times. As performance measure, the relative root-mean-square error (RMSE) is determined with $\mathrm{RMSE}_\alpha = ((1/k)\sum_{n=1}^{k}(\tilde{\alpha} - \alpha)^2/\alpha)^{1/2}$. Likewise, RMSE_{σ^2} is calculated.
3) In order to investigate the effect of an erroneously estimated $\tilde{\boldsymbol{h}}_t$ on the accuracy of the succeeding estimations of $\tilde{\alpha}_{t+1}$ and $\tilde{\sigma}^2_{t+1}$, the power $\mathbf{P}$ for various heart locations with radial distance $\|\mathbf{h}\|$ and uniformly distributed azimuth angle is simulated. An error is added to $\mathbf{h}$ which then constitutes the estimate $\tilde{\mathbf{h}}$ which is used for the estimation of the nuisance parameters. For increasing error, the nuisance parameters are estimated. In this simulation, the power values are calculated using a constant scaling parameter $\alpha = 1$ and noise parameter $\sigma^2 = 0$ ($\mathrm{SNR} = \infty$).

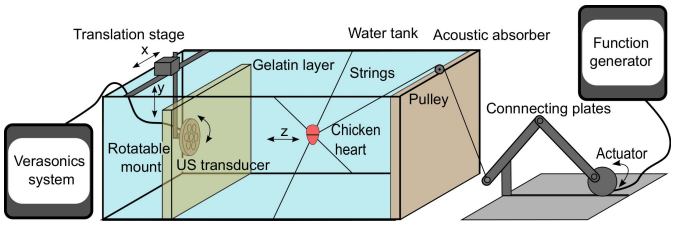

Fig. 5. Schematic of the fetal heart *in vitro* setup. A function generator drives an actuator which is connected via a string to a chicken heart. In that way, the chicken heart is moved along the z-direction in a beatlike fashion. By translating the US transducer through the water tank, displacement of the heart out of the measurement range of the transducer can be mimicked.

I. In Vitro Measurements

In order to evaluate the performance experimentally, an *in vitro* beating fetal heart setup was built (see Fig. 5), which can be used to mimic a changing fHL with respect to the US transducer.

This setup consists of a US transducer attached to a rotatable mount which can be moved using a translation stage. The beating fetal heart is represented by a chicken heart threaded on 5-μm-thick fishing strings, which are attached to the wall of the water tank at an adjustable distance to hold the heart in a fixed position. The reason for using a chicken heart is motivated by the requirement of having similar dimensional and acoustical properties to those of a human fetal heart. It is known that the biventricular outer diameter of the fetal heart varies between 0.9 and 3.9 cm for gestational age of 14–40 weeks [14]. In the conducted experiments, the dimensions of the chicken heart are comparable.

A beatlike pattern is created by attaching another fishing string to the heart which goes via a pulley to a connecting plate. This plate is brought into motion by an actuator such that the fishing string is pulled backward to create a displacement of the chicken heart along the z-direction. A function generator allows to tune the frequency and the displacement of the actuator. In the conducted experiments, the heart rate was set to 140 beats per minute which is a typical fHR measured during labor [19]. Furthermore, the displacement of the chicken heart was tuned such that it corresponds to the distance covered by the fetal cardiac wall during one heartbeat, i.e., $d_z = 5$ mm [5].

It was hypothesized that the EKF would work better in high noise scenarios compared to the ML estimation approach. Because the experiments are performed in a water tank effectively, limited acoustic attenuation is taking place. However, *in vivo* acoustic attenuation is a nonnegligible factor affecting the SNR. It becomes especially relevant for measurements on women with a high BMI. In order to mimic a reduced SNR, the transducer elements are driven with a very low driving voltage of 5 V. Furthermore, a tissue mimicking gelatin-water phantom was placed between the US transducer and the chicken heart. The gelatin concentration was 15%, and 0.1% of 10 μm Al_2O_3 was added as acoustic scatterer.

An example of a Doppler signal measured using a commercially available CTG US transducer in the *in vitro* setup is shown in Fig. 1. Due to the fact that the beating fetal heart is reduced to an object, i.e., the chicken heart, which only moves along one direction, the measured Doppler signals do not have the contribution of the contracting heart ventricles, closing valves or blood flow [20]. However, the Doppler signals measured using this setup are by visual inspection very similar to *in vivo* measurements reported in [10] and [18].

The transducer was aligned with respect to the chicken heart such that the chicken heart was positioned in front of the center element at depth $h_z = 80$ mm, which is a typical depth at which the fetal heart is located within the maternal abdomen. A drift of the fetal heart out of the radiation pattern of the US transducer at moderate velocity is then simulated by translating the US transducer through the water tank at velocity $u = 1.5$ mm/s. After each measurement, the US transducer is rotated by an angle of 45° in order to investigate the performance for multiple heart locations. In total, 33 measurements were conducted.

III. Results

A. Simulations

An illustrative example of the fetal heart localization performance is depicted in Fig. 6 based on the simulated data. In this simulation, the fetal heart changes its location according to the trajectory in the left of Fig. 6(a) at depth $h_z = 80$ mm. In the right of Fig. 6(b), the corresponding simulated power measurements at SNR $= -5$ dB are shown. When the fetal heart is located in front of a specific element, that specific element receives a relatively high power compared to the other elements. It should be noted that, as discussed in Section II-G, only the center element is used for transmission. This is reflected by the fact that when the fetal heart is located in front of the center element, the received power is higher compared to the situation when the fetal heart is located in front of one of the other elements.

In the top of Fig. 6(b), it is visible how $\|\mathbf{KG}\|$ evolves during the EKF iterations. When the fetal heart moves out of the center of the radiation pattern, $\|\mathbf{KG}\|$ reduces, meaning that new power measurements will contribute less to the estimation of $\tilde{\mathbf{h}}$ and more weight is given to its *a priori* estimate. This is the expected behavior of the EKF, as the SNR reduces when the fetal heart is drifting out of the radiation pattern. Correspondingly, the norm of the state variance $\|\mathbf{S}\|$ increases, as visible in the second panel of Fig. 6(b), which reflects our increasing uncertainty about the current estimate.

In the lower two panels, the results of the estimation are shown and compared to the ML approach. It can be seen that the estimate $\tilde{\mathbf{h}}$ reliably follows the real fHL $\mathbf{h}$. While the EKF is able to cope with the reduced SNR when the fetal heart drifts out of the radiation pattern, the ML estimator shows large errors.

In Fig. 7, the results of the simulations to evaluate the effect of $\|\mathbf{Q}\|$ on the estimation accuracy are shown (simulation 1). The three graphs show the error of the estimation as a function of the process noise variance and varying SNR for three different velocities. From the graphs, it follows that for a specific velocity u, there is an optimal setting for the process noise variance. The process noise variance, in fact, determines how much the fHL is expected to change from one-time point to the other. On the one hand, when set too low, one does not permit enough movement to the fetal heart. As a consequence, the estimate will remain at its initial value and cannot adapt according to the new measurement data. On the other hand, when the process noise variance is set too high, large changes of the fHL are permitted and the system follows only the measurement data. Setting the process noise to large values compared to the present measurement noise variance $\mathbf{R}$ effectively changes the EKF to an ML approach as one removes virtually any prior knowledge. For realistic velocities with which the fetal heart moves out of the radiation pattern, the results in Fig. 7 suggest that a process noise variance with a magnitude in the range of $\|\mathbf{Q}\| = 1 - 100$ is a good tradeoff.

After each EKF iteration step, the nuisance parameters $\tilde{\alpha}$ and $\tilde{\sigma}^2$ are again estimated to be available for the next estimation of $\tilde{\mathbf{h}}$ and $\tilde{\mathbf{S}}$. Fig. 8 shows the RMSE as function of the radial distance $\|\mathbf{h}\|$ and different SNRs (simulation 2). Not surprisingly, the estimation accuracy for both nuisance parameters decreases for decreasing SNR. However, when comparing the RMSE values for α and σ^2, two aspects stand out. First, the RMSE for the estimation of α is much larger compared to RMSE_{σ^2}. Second, with increasing radial distance $\|\mathbf{h}\|$, the estimation accuracy of α drastically worsens, while the estimation accuracy of σ^2 is less affected.

In Fig. 9, the effect of an erroneous estimated fHL $\tilde{\mathbf{h}}_t$ on the following estimation of $\tilde{\alpha}_{t+1}$ and $\tilde{\sigma}^2_{t+1}$ is depicted (simulation 3). As expected, when there is no estimation error,

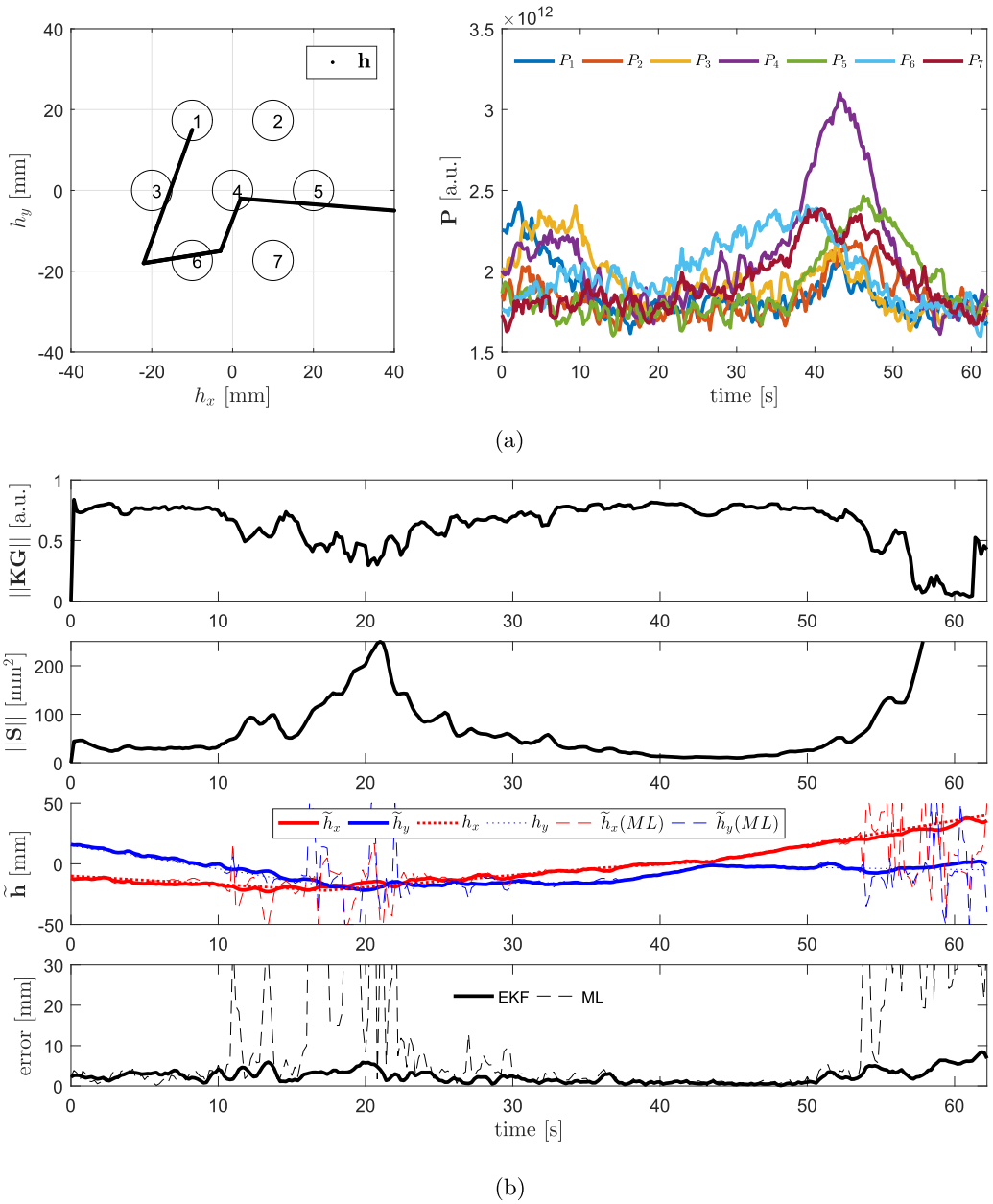

Fig. 6. Illustrative example of the performance of the hierarchical EKF algorithm on simulated power measurements for a changing fHL. (a) Spatial representation of a simulated trajectory of the fetal heart $\mathbf{h}$ (left) and simulated power measurements P_i for the individual transducer elements (right). The scaling parameter is set to an arbitrary chosen value $\alpha = 3.1 * 10^{12}$ and the SNR was set to SNR $= -5$ dB. Note that only the center element is used for transmission. (b) From top to bottom graph: Evolution of the norm $\|\mathbf{KG}\|$; Evolution of the norm of the state variance $\|\mathbf{S}\|$; fHL estimation $\tilde{\mathbf{h}}$ obtained with the EKF algorithm. For reference, the real fHL h and the results of the ML estimation $\tilde{\mathbf{h}}$(ML) are presented; Error of the fHL estimation using the EKF and ML approach.

both nuisance parameters can be estimated perfectly because the SNR in the simulation was set to infinity. With increasing error, the nuisance parameter estimation accuracy is reduced. It strikes that for a small error $= 5$ mm, RMSE$_\alpha$ can already be significant. Further increasing the error to 15 mm even leads to RMSE$_\alpha$ of 37% in the center of the radiation pattern. For σ^2, RMSE$_{\sigma^2}$ is also increasing when $\tilde{\mathbf{h}}$ is estimated more inaccurately. With increasing radial distance $\|\mathbf{h}\|$, RMSE$_{\sigma^2}$ is less affected by an erroneously estimated fHL. It should be noted that the bottom of Fig. 9 shows absolute values instead of a relative RMSE because $\sigma^2 = 0$.

B. In Vitro Experiments

The results of the *in vitro* measurements are shown in Fig. 10. The estimation error of the EKF is compared to the ML approach. For reference, the results of the EKF on simulated data are also presented. In these simulations, the fHL changes in the same way as in the conducted *in vitro* experiments.

Within the measurement volume of the US transducer, there is no significant difference between the error of the fHL estimation obtained with the EKF algorithm compared to the ML approach. Only when the fetal heart is moving out of the

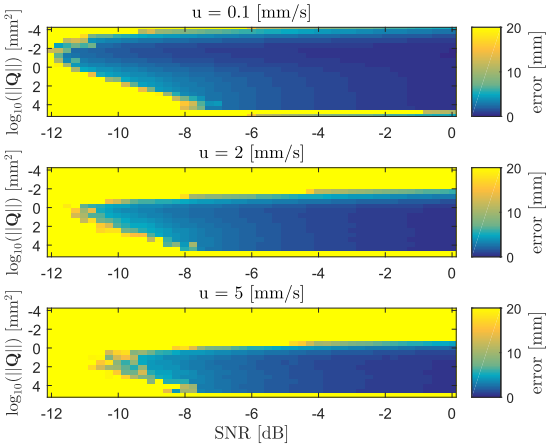

Fig. 7. Influence of the set magnitude of the process noise variance $\|\mathbf{Q}\|$ on the fHL estimation accuracy for varying SNR. In the simulation, the trajectory of the fetal heart moves two times around the center of the radiation pattern at a constant radial distance $\|\mathbf{h}\|$. The simulations are done for different velocities u, representing a slow, a moderate, and a fast-changing fHL. The color coding represents the mean error of the fHL estimation.

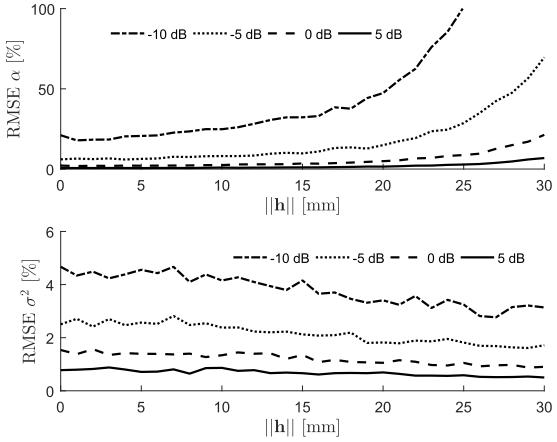

Fig. 8. RMSE of the estimation of the nuisance parameters α and σ^2 as function of an increasing radial distance $\|\mathbf{h}\|$ for four different SNRs. The depth of the fetal heart was set to $h_z = 80$ mm.

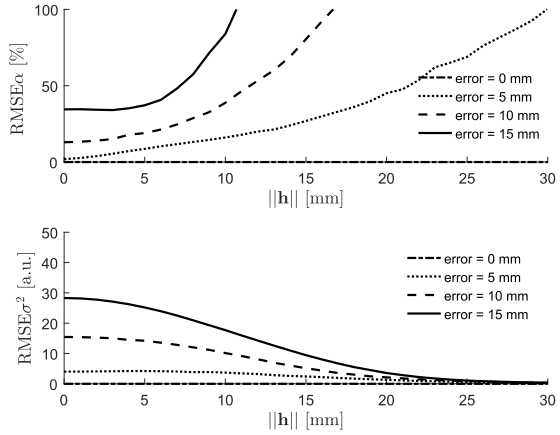

Fig. 9. RMSE of the nuisance parameter estimation as function of an increasing radial distance $\|\mathbf{h}\|$. Successively, an error is added to the real fHL $\|\mathbf{h}\|$ which is then used as the fHL estimate for the nuisance parameter estimation.

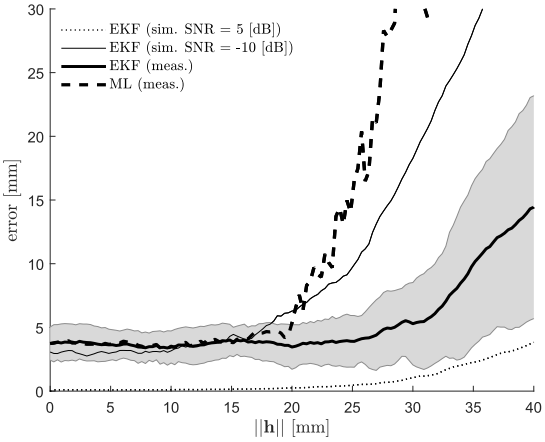

Fig. 10. Performance of the EKF compared to ML obtained from *in vitro* measurements. For reference, the EKF results on simulated data with SNR = 5 dB and SNR = −10 dB are presented. The shaded gray area represents the standard deviation of the error using the EKF. Simulations and measurements are conducted at a depth of $h_z = 80$ mm.

radiation pattern at a radial distance $\|\mathbf{h}\| = 20$ mm, the performance of the ML approach drastically reduces. Compared to that, the EKF is able to estimate the fHL over a considerably wider measurement range. The diameter and the pitch of the transducer elements are 10 mm, which determine the required accuracy of the fetal heart localization. With this accuracy, one is able to determine on which side of the radiation pattern the fetal heart is located. Considering this as the required accuracy, the measurement range is increased by 41%.

Furthermore, it can be recognized that, within the radiation pattern, the estimation error during the measurements is approximately 4 mm for both the EKF and ML approach, while for the simulations performed at SNR = −10 dB, the error for the EKF is lower. However, as $\|\mathbf{h}\|$ increases, the error in the simulations increases faster compared to the *in vitro* measurements.

IV. Discussion

Positioning the US transducer on the maternal abdomen requires skill and can be a tedious task. By estimating the fHL during Doppler fHR measurements, a visual feedback to assist with the transducer positioning can be provided. It allows positioning of the US transducer centrally above the fetal heart, reducing the change that the fetal heart moves out of the US beam. Besides an improvement of the clinical workflow, this may also reduce the total amount of fHR signal loss periods, hence, contributing to the improved assessment of the fetal condition. The added value of the proposed US transducer positioning tool needs to be further validated in a clinical study. Here, an important outcome measure is the required time clinicians need to position the US with and without positioning support. In addition, it is important to investigate whether inexperienced nurses, or potentially even the mother-to-be, have less difficulties to position the US transducer.

Although the proposed method may lead to improved clinical workflow, the clinically more relevant parameter is the fHR. It needs to be evaluated if and how much the robustness of the fHR recordings will improve due to the proposed US transducer positioning tool. Although we are convinced that the proposed method will positively affect the robustness of

fHR recordings, at this stage, it can only be conjectured if this is really the case. Therefore, it is essential to prove the impact of the method in a clinical setting.

From the results shown in Fig. 8, it is clear that the estimation of the nuisance parameters is strongly affected by the SNR. Specifically, α is more affected by a decreasing SNR compared to σ^2. While α is a parameter belonging to the signal component of the model, σ^2 describes the noise. Therefore, it is logical that when noise is dominating the signal α can be less accurately determined while the estimate for σ^2 is independent of the signal itself.

The results in Fig. 9 stress the importance of a good initialization of the EKF. When $\tilde{\mathbf{h}}$ is erroneous, the subsequent nuisance parameter estimation will potentially show large errors, which in turn lead to a misuse of the model in the following EKF iteration. It can be seen that with increasing radial distance $\|\mathbf{h}\|$, errors in $\tilde{\mathbf{h}}$ have less impact on the estimation on σ^2. This can be explained by the fact that the model $\Phi(\mathbf{h})$ approaches zero at increasing radial distance and the gradient is very small. Therefore, an erroneous $\tilde{\mathbf{h}}$ will cause a smaller error in $\Phi(\mathbf{h})$. In contrast to that, as α belongs to the signal component of the model, it is crucial that some signal needs to be measured for a good estimation of $\tilde{\alpha}$. For the envisioned application, this implies that the heart location has to be already approximately known when the transducer is positioned on the maternal abdomen, such that the nuisance parameters can be estimated correctly.

As it can be seen in Fig. 10, there is no performance difference between the EKF and ML approach when the fetal heart is located at a minimum radial distance $\|\mathbf{h}\| = 16$ mm from the center of the radiation pattern. This can be explained by the high SNR within the center of the US beam. Here, a small nuisance parameter σ^2 will cause that the measurement noise covariance matrix $\mathbf{R}$ converges toward the zero matrix [see (14)]. This has an effect that the EKF will almost fully rely on new incoming measurement data and will disregard the prior knowledge, causing the fHL estimation result to be similar to the ML approach.

The advantage of the EKF compared to the ML lies particularly in an improved performance when the fetal heart is moving out of the radiation pattern or the SNR drops during measurements. Therefore, in a practical implementation of the proposed algorithm, while searching for the fHL, one could first rely on the ML estimation and then switch to the EKF for improved tracking of the fHL. This switch could be initiated by the operator or automatically triggered when the system is able to estimate the fHR. Comparison between the performance of the EKF *in vitro* and *in silico* (see Fig. 10) suggests that the SNR in the experiments is between the range of SNR $= -10$–5 dB. Interestingly, within the center of the radiation pattern, the performance of the simulation carried out at SNR $= -10$ dB is slightly better than for the *in vitro* measurements. This can be explained by a misalignment of the chicken heart and the transducer in the experimental setup. Furthermore, it may also reflect the inaccuracy in our power model and possible limitations of the applied assumptions.

The setting for the process noise variance $\mathbf{Q}$ plays an important role in the performance of the EKF, which can be clearly seen in Fig. 7. The ratio between the process noise variance $\mathbf{Q}$ and the measurement noise variance $\mathbf{R}$ determines the magnitude of the Kalman gain $\mathbf{K}$, and therefore, how much the system relies on the old estimate $\tilde{\mathbf{h}}$ or the new measurement data. The optimal setting for $\|\mathbf{Q}\|$ is selected when the system can just follow the maximal velocity with which the fHL changes. Setting $\|\mathbf{Q}\|$ too high pushes the EKF toward the ML approach, because it effectively sets the prior to a uniform probability. However, it should be noted that setting a too low $\|\mathbf{Q}\|$ is more disadvantageous since it does not allow the system to adjust to the new measurement data. For further improvement of the fHL estimation algorithm, it can be considered to adaptively estimate the process noise variance [4], [15]. In addition, a second-order Gauss–Markov model for the state-space representation in (3), i.e., including knowledge on the movement direction of the fetal heart, could potentially improve the estimation [15].

In the derivation of the EKF algorithm, we assumed that, by modeling the process noise with a first-order Gauss–Markov process, the probability of the moving direction of the fetal heart is equally alike for all directions. Therefore, from the process perspective, the method itself is not affected by the moving direction of the fetal heart. However, as discussed before, a low SNR may lead to an erroneous estimation of the model parameters. This means that when the fetal heart moves from a location where the SNR is low, i.e., outside the US beam, toward the center of the beam, the performance of the method will be reduced compared to the situation where the heart moves from a location with good to locations with poor SNR. Furthermore, in this research the simulations and experiments were performed for one representative depth $h_z = 80$ mm and the SV of the acquisition was set accordingly. In a clinical situation, the fetal heart may not only drift outside the radiation pattern but also change its depth. Further research is needed to automatically adjust the SV (gate) to the depth of the fHL. The performance of the fHL estimation algorithm in such a situation needs to be analyzed.

The experimental setup allows mimicking a displacement of the fetal heart with respect to the US transducer. Furthermore, by adding a gelatin phantom, the US waves can be attenuated to simulate measurements in women with high BMI. However, it is well-known that the US Doppler signals may be affected by pulsating maternal arteries or artifacts caused by fetal limb movement [12], [16]. This will have an effect on the measured Doppler signals and Doppler power, hence, influencing the performance of the fHL estimation. In the future research, the measurement system will be extended to mimic these sources of signal distortion and it will be investigated how the proposed method can work robustly in these situations. In particular, a research topic is the acquisition of Doppler signals from multiple depths, allowing spatial separation of different Doppler sources.

For an accurate estimation of the fHL, it is necessary that the SNR is sufficiently high. Obviously, the SNR reduces as the fetal heart moves out of the radiation pattern. In order to increase the measurement volume, the size of the transducer elements or the center frequency of the transmit pulse can be reduced. This leads to a wider radiation pattern. In the current

research, only the center element of the transducer was used because transmission with all elements leads to a radiation pattern with strong interference and finding an analytical solution for the nonlinear mapping function $\mathbf{g}$ would, hence, be more challenging. Further research on the transducer design and the transmitted radiation pattern needs to be conducted. By changing the size of the transducer elements, a US wave could be transmitted which is closer to a plane or diverging wave, spanning a wider measurement range. In addition to that, with a new transducer design in which the pitch between the transducer elements is reduced, the transmitted US beam can potentially be steered into the direction of the fetal heart. Having a system which would be able to automatically steer the beam toward the fHL, the fHR estimation may be less influenced by the correct positioning of the US transducer by the clinical staff.

V. Conclusion

In this research, a new method for estimating the fHL during Doppler-based fHR monitoring is presented, which facilitates improved US transducer positioning on the maternal abdomen. The method makes use of a model which relates the Doppler power, measured in the individual transducer elements of a commercially available US transducer, to the fHL. This novel model is used in the framework of an EKF, where the model parameters are estimated in an adaptive way. This allows estimating the fHL in high noise scenarios. The performance of the algorithm was analyzed in *in silico* and in *in vitro* using a dedicated experimental fetal beating heart setup, and compared to an ML estimation approach. The results show that the fHL can be determined with an accuracy of 4 mm when the fetal heart is located within the measurement range of the transducer. It was proven that the EKF is suitable to estimate the fHL more accurately in high noise scenarios as compared to an ML approach. In the experiments, when the fetal heart drifts out of the measurement range, the EKF algorithm is able to accurately estimate the fHL up to a radial distance of $\|\mathbf{h}\| = 34$ mm, while the ML approach can only determine it up to $\|\mathbf{h}\| = 24$ mm. This corresponds to an increase in the measurement range by 41%. The improved performance of the method shows the feasibility of fHL estimation, even in measurements with low SNR. Eventually, this may lead to improved US transducer positioning for improved clinical workflow and more robust estimation of the fHR.

Acknowledgment

This paper was performed within the framework of IMPULS perinatology.

References

[1] F. Andreotti *et al.*, "Maternal signal estimation by Kalman filtering and template adaptation for fetal heart rate extraction," in *Proc. Comput. Cardiol.*, vol. 40, Sep. 2013, pp. 193–196.

[2] D. Ayres-de Campos and J. Bernardes, "Twenty-five years after the FIGO guidelines for the use of fetal monitoring: Time for a simplified approach?" *Int. J. Gynecology Obstetrics*, vol. 110, no. 1, pp. 1–6, 2010.

[3] R. S. Cobbold, "Pulsed methods for flow velocity estimation and imaging," in *Foundations of Biomedical Ultrasound*. Oxford, U.K.: Oxford Univ. Press, 2007, ch. 10, pp. 652–712.

[4] J. F. G. de Freitas, M. Niranjan, and A. H. Gee. "'Hierarchical Bayesian-Kalman models for regularisation and ARD in sequential learning," Dept. Eng., Cambridge Univ. Dept. Eng., U.K., Tech. Rep. CUED/F-INFENG/TR 307, Dec. 1997.ember 1997.

[5] N. N. Elmstedt *et al.*, "Reference values for fetal tissue velocity imaging and a new approach to evaluate fetal myocardial function," *Cardiovascular Ultrasound*, vol. 11, no. 1, p. 29, 2013.

[6] S. Fischer, P. Schmitt, D. Ensminger, F. Abda, and A. Pallares, "A new velocity estimation method using spectral identification of noise," *Flow Meas. Instrum.*, vol. 19, nos. 3–4, pp. 197–203, 2008.

[7] P. Hamelmann *et al.*, "Ultrasound transducer positioning aid for fetal heart rate monitoring," in *Proc. 38th Annu. Int. Conf. IEEE Eng. Med. Biol. Soc. (EMBC)*, Orlando, FL, USA, Aug. 2016, pp. 4105–4108.

[8] P. Hamelmann *et al.*, "Improved ultrasound transducer positioning by fetal heart location estimation during Doppler based heart rate measurements," *Physiological Meas.*, vol. 38, no. 10, pp. 1821–1836, Sep. 2017.

[9] Jensen, *Estimation of Blood Velocities Using Ultrasound: A Signal Processing Approach*. Cambridge, U.K.: Cambridge Univ. Press, 1996.

[10] J. Jezewski, D. Roj, J. Wrobel, and K. Horoba, "A novel technique for fetal heart rate estimation from Doppler ultrasound signal," *Biomed. Eng. OnLine*, vol. 10, no. 1, p. 92, 2011.

[11] L. Kleeman, "Understanding and applying Kalman filtering," in *Proc. 2nd Workshop Perceptive Syst., Curtin Univ. Technol.*, Perth, WA, Australia, 1996, p. 17.

[12] A. Kribèche, F. Tranquart, D. Kouame, and L. Pourcelot, "The Actifetus system: A multidoppler sensor system for monitoring fetal movements," *Ultrasound Med. Biol.*, vol. 33, no. 3, pp. 430–438, 2007.

[13] L. M. Leemis and J. T. McQueston, "Univariate distribution relationships," *Amer. Statistician*, vol. 62, no. 1, pp. 45–53, 2008.

[14] S. Luewan, Y. Yanase, F. Tongprasert, K. Srisupundit, and T. Tongsong, "Fetal cardiac dimensions at 14-40 weeks' gestation obtained using cardio-STIC-M," *Ultrasound Obstetrics Gynecology*, vol. 37, no. 4, pp. 416–422, 2011.

[15] R. K. Mehra, "On the identification of variances and adaptive Kalman filtering," *IEEE Trans. Autom. Control*, vol. AC-15, no. 2, pp. 175–184, Apr. 1970.

[16] M. L. Murray, "Maternal or fetal heart rate? Avoiding intrapartum misidentification," *J. Obstetric, Gynecologic, Neonatal Nursing*, vol. 33, no. 1, pp. 93–104, 2004.

[17] D. Paladini, "Sonography in obese and overweight pregnant women: Clinical, medicolegal and technical issues," *Ultrasound Obstetrics Gynecology*, vol. 33, no. 6, pp. 720–729, 2009.

[18] C. H. L. Peters *et al.*, "Beat-to-beat detection of fetal heart rate: Doppler ultrasound cardiotocography compared to direct ECG cardiotocography in time and frequency domain," *Physiological Meas.*, vol. 25, no. 2, pp. 585–593, Apr. 2004.

[19] S. P. von Steinburg *et al.*, "What is the 'normal' fetal heart rate?" *PeerJ*, vol. 1, p. e82, Jun. 2013.

[20] S. Shakespeare, J. A. Crowe, B. R. Hayes-Gill, K. Bhogal, and D. K. James, "The information content of Doppler ultrasound signals from the fetal heart," *Med. Biol. Eng. Comput.*, vol. 39, no. 6, pp. 619–626, Feb. 2001.

[21] M. G. Signorini, A. Fanelli, and G. Magenes, "Monitoring fetal heart rate during pregnancy: Contributions from advanced signal processing and wearable technology," *Comput. Math. Methods Med.*, vol. 2014, Jan. 2014, Art. no. 707581.

[22] I. Voicu, J.-M. Girault, C. Roussel, A. Decock, and D. Kouame, "Robust estimation of fetal heart rate from US Doppler signals," *Phys. Procedia*, vol. 3, no. 1, pp. 691–699, Jan. 2010.

Paul Hamelmann was born in Freiburg im Breisgau, Germany, in 1988. He received the M.Sc. degree in biomedical engineering from the University of Twente, Enschede, The Netherlands, in 2013. He is currently pursuing the Ph.D. degree with the BM/d Team, Signal Processing Group, Eindhoven University of Technology, Eindhoven, The Netherlands.

He is involved in the improvement of fetal heart rate monitoring using Doppler ultrasound, in corporation with Philips Research, Eindhoven, and the Maxima Medical Center, Eindhoven.

Rik Vullings received the M.Sc. degree (Hons.) in applied physics and the Ph.D. degree in electrical engineering, with a focus on analysis and interpretation of the noninvasive fetal electrocardiogram, from the Eindhoven University of Technology (TU/e), Eindhoven, The Netherlands, in 2005 and 2010, respectively.

He was a Post-Doctoral Researcher with TU/e, where he was appointed as an Assistant Professor in 2013. In 2009, he founded the spin-off company Nemo Healthcare, Veldhoven, The Netherlands, where he is currently the CSO. His current research interests include model-based biomedical signal processing with applications in perinatology, cardiology, and somnology.

Massimo Mischi (M'02–SM'10) received the M.Sc. degree in electrical engineering from La Sapienza University, Rome, Italy, in 1999, and the Ph.D. degree from the Eindhoven University of Technology (TU/e), Eindhoven, The Netherlands, in 2004.

In 2007, he was an Assistant professor with the Electrical Engineering Department, TU/e. In 2011, he was an Associate Professor with TU/e and founded the Biomedical Diagnostics Research Laboratory, where he was involved in model-based quantitative analysis of biomedical signals with applications ranging from electrophysiology to diagnostic imaging. He is currently a Full Professor with the Electrical Engineering Department, TU/e. He was a recipient of the STW VIDI Grant in 2009 and with the ERC Starting Grant in 2011 for his research on angiogenesis imaging. He has co-authored more than 250 peer-reviewed publications and several book chapters. He holds 11 patents.

Dr. Mischi is the Chairman of the IEEE EMBS Benelux Chapter. He is also the Board Member of the Imaging Section of the European Association of Urology and Secretary of the Dutch Society of Medical Ultrasound.

Alexander F. Kolen received the Ph.D. degree from the Institute of Cancer Research, University of London, London, U.K., in 2003.

Since 2003, he has been with Philips Research, Eindhoven, The Netherlands, leading several cardiac US-related projects. From 2004 to 2005, he held a post-doctoral position with Maastricht University, Maastricht, The Netherlands, where he was involved in the analysis of cardiac mechanic using tissue Doppler US. His current research interests include ultrasound (US) diagnosis of liver tumors, followed by monitoring high-intensity focused US treatment based on US elastography.

Lars Schmitt received the Dr.-Ing. degree in electrical engineering from Ruhr-Universität Bochum, Bochum, Germany, in 2001, and the Ph.D. degree in information technology from RWTH Aachen University, Aachen, Germany, in 2008.

He was involved in the field of medical device research and patient care technology innovation with Philips, Eindhoven, The Netherlands. In 2017, he joined Grünenthal, Aachen, as an International Technical Project Lead for digital health.

Jan W. M. Bergmans received the M.Sc. and Ph.D. degrees in electrical engineering from the Eindhoven University of Technology (TU/e), Eindhoven, The Netherlands, in 1981 and 1987, respectively.

From 1981 to 1982, he was a Manager of communication projects with the Royal Netherlands Navy, Den Helder, The Netherlands. From 1982 to 1999, he was with the Philips Research Laboratories, Eindhoven. From 1988 to 1989, he was an Exchange Researcher with the Digital Video Recording Group, Hitachi Central Research Laboratories, Tokyo, Japan. From 1991 to 1999, he co-led the Research and Development Team, Philips Research Laboratories, where he was involved in the development of signal processing techniques and integrated circuits for data storage systems. In 1999, he was a Full Professor with TU/e and the Chair of the Signal Processing Systems Group, TU/e. In 2000, he became a Scientific Advisor with the Philips Research Laboratories. Since 2006, he has been the Co-Manager with BrainBridge, Eindhoven, the strategic collaboration between TU/e, the Philips Research Laboratories, and Zhejiang University, Hangzhou, China.